CELL CYCLE
2023, VOL. 22, NO. 9, 1116–1126
https://doi.org/10.1080/15384101.2023.2178102

Taylor & Francis
Taylor & Francis Group

Check for updates

HRD1 functions as a tumor suppressor in ovarian cancer by facilitating ubiquitination-dependent SLC7A11 degradation

Yanyan Wang, Shanfeng Wang, and Wenjuan Zhang

Department of obstetrics and gynecology, The First Affiliated Hospital of Jinzhou Medical University, Jinzhou, China

ABSTRACT

The E3 ubiquitin ligase 3-hydroxy-3-methylglutaryl reductase degradation (HRD1) was found to be a tumor suppressor in diverse types of cancers; we aimed to explore its expression pattern and biological function in ovarian cancer (OC). HRD1 expression in OC tumor tissues was detected using quantitative real-time polymerase chain reaction (qRT-PCR) and immunohistochemistry (IHC). The overexpression plasmid of HRD1 was transfected into OC cells. Cell proliferation, colony formation, and apoptosis were analyzed using bromodeoxy uridineassay, colony formation assay, and flow cytometry, respectively. OC mice models were established to explore the effect of HRD1 on OC *in vivo*. Ferroptosis was evaluated by malondialdehyde, reactive oxygen species, and intracellular ferrous iron. Expressions offerroptosis-related factors were examined using qRT-PCR and western blot. Erastin and Fer-1 were, respectively, employed to promote or inhibit ferroptosis in OC cells. Online bioinformatics tool and co-immunoprecipitation assay were performed to predict and verify the interactive genes of HRD1 in OC cells, respectively. Gain-of-function studies were carried out to determine the roles of HRD1 in cell proliferation, apoptosis, and ferroptosis *in vitro*. HRD1 was under-expressed in OC tumor tissues. The overexpression of HRD1 inhibited OC cell proliferation and colony formation *in vitro* and suppressed OC tumor growth *in vivo*. The overexpression of HRD1 promoted cell apoptosis and ferroptosis in OC cell lines. HRD1 interacted with the solute carrier family 7 member 11 (SLC7A11) in OC cells, and HRD1 regulated the stability and ubiquitination in OC. SLC7A11 overexpression recovered the effect of HRD1 overexpression in OC cell lines. HRD1 inhibited tumor formation and promoted ferroptosis in OC through enhancing SLC7A11 degradation.

ARTICLE HISTORY
Received 2 July 2022
Revised 15 September 2022
Accepted 5 January 2023

KEYWORDS
HRD1; ovarian cancer; ferroptosis; SLC7A11; ubiquitination

Introduction

Ovarian cancer (OC) is one of the three most common malignant tumors of female reproductive organs worldwide [1], which has the highest mortality rate among all kinds of gynecological tumors [2]. Globally, approximately 313,959 women are diagnosed with OC, resulting in 207,252 deaths per year [3]. Despite the rise of great advancements in therapeutic strategies for OC patients, including surgery, radiotherapy, and chemotherapy, the 5-year survival rate of OC is still unsatisfied [4]. Therefore, to explore the molecular mechanisms and to find potential targets are urgently needed for OC diagnosis and therapy.

Ferroptosis is a novel form of iron-dependent programmed cell death [5]. It is well documented that targeting ferroptosis might be a potential strategy for cancer therapy, including OC [6]. Solute carrier family 7 member 11 (SLC7A11) is a cystine/glutamic acid Xc-transport carrier responsible for the specific transport of cystine and glutamine and acts as the rate-limiting precursor for glutathione (GSH) biosynthesis [7]. SLC7A11 has been reported to be overexpressed and associated with poor prognosis in diverse cancers including OC [8]. Moreover, SLC7A11, as a key suppressor of ferroptosis, has been reported to play a role in inhibiting ferroptosis in OC [9,10]. Therefore, in-depth insights into the regulatory mechanisms of SLC7A11-mediated ferroptosis in tumor metabolism could provide us with important clues for OC treatment.

3-Hydroxy-3-methylglutaryl reductase degradation (HRD1), also called synoviolin, is an E3 ubiquitin ligase involved in endoplasmic reticulum-associated degradation (ERAD) by promoting the

CONTACT Wenjuan Zhang zhangwenjuan6668@jzmu.edu.cn Department of obstetrics and gynecology, The First Affiliated Hospital of Jinzhou Medical University, No.2 Renmin Street, Jinzhou 121001, China

© 2023 Informa UK Limited, trading as Taylor & Francis Group

degradation of misfolded proteins [11,12]. Previous studies have shown that HRD1 functions as a tumor suppressor in breast cancer [13–15]. On the contrary, the tumor-promoting effects of HRD1 have been revealed in colon cancer [16], lung cancer [17], and hepatocellular carcinoma [18]. However, its involvement in OC tumorigenesis remains unknown.

In the present study, we detected the expression level of HRD1 in OC. Furthermore, we explored the effects of HRD1 on the cell proliferation, growth, and ferroptosis of OC *in vivo* and *in vitro*. Before conducting the experiment, a predicted binding site between SLC7A11 and HRD1 was found on the UbiBrowser bioinformatics website (http://ubibrowser.ncpsb.org/ubibrowser/home/index), indicating a potentially regulatory effect of HRD1 on SLC7A11. Considering the importance of SLC7A11 in ferroptosis, we speculated that HRD1 might be involved in the regulation of ferroptosis, which accounted for its role in OC. The goal of this study is to clarify the connection between HRD1, ferroptosis, and OC and to uncover the potential regulatory mechanism.

Materials and methods

Human tissue samples and clinical data

OC tumor tissue samples ($n = 15$) and nonmalignant ovarian tissue samples ($n = 15$) were harvested from The First Affiliated Hospital of Jinzhou Medical University between October 2011 and April 2018 from OC patients. The inclusion criteria were as follows: patients ≥ 18 years of age with newly diagnosed advanced, high-grade epithelial ovarian, primary peritoneal, or fallopian tube cancer who have achieved a response after completion of cytoreductive surgery, and initial platinum-based chemotherapy are enrolled. The exclusion criteria were as follows: patients with other metastatic tumors and/or those who had received prior chemoradiotherapy or radiotherapy. The clinical characteristics of OC patients are listed in Table 1. The tumor stage was identified using the International Federation of Gynecology and Obstetrics (FIGO) staging system, while the histological grades were determined according to the World Health Organization's Histological Grading System. Besides, the lymph node status of these patients was assessed by lymph node dissection. The 15 cases of nonmalignant ovarian tissue samples were obtained from patients with benign uterine disease with normal ovaries that were subjected to oophorectomy in our hospital. This study was approved by the Guidelines of The First Affiliated Hospital of Jinzhou Medical University and performed according to the ethical guidelines of the Declaration of Helsinki (approval number: NO.202133). Written informed consent was achieved from all patients.

Table 1. The clinical characteristics of OC patients ($n = 15$).

Parameters	Number of cases	HRD1 expression		*P* value
		Low ($n = 7$)	High ($n = 8$)	
Age				>0.05
<60	5	2	3	
≥60	10	5	5	
Tumor stage				<0.05
I–II	10	2	8	
III–IV	5	4	1	
Lymph node metastasis				<0.05
No	8	2	6	
Yes	7	5	2	

Immunohistochemistry (IHC) staining

The expression level of HRD1 in clinically respected tissue samples was evaluated using IHC staining. Briefly, tissue specimens (three samples per group) were randomly selected and embedded in paraffin after being fixed with neutral buffered formalin (10%). The tissue specimens were then cut into 4-μm sections and rested on silane-coated slides. The slides were subsequently deparaffinized, and the slide sections were incubated with H_2O_2 (3%) followed by blocking with bovine serum albumin (5%, BSA). Then, HRD1 primary antibody (Abcam, Cambridge, MA, USA) was applied to treat the sections at 4°C overnight. After that, a horseradish peroxide-conjugated secondary antibody (Abcam, USA) was employed to incubate the slides for 30 min at 37°C. Next, 3,3′-diaminobenzidine (DAB) solution and hematoxylin were, respectively, used for staining and counterstaining these slides.

Cell culture

Two OC cell lines (A2780 and SKOV3) were provided by BeNa Culture Collection (Beijing, China). Roswell Park Memorial Institute-1640 medium (Sigma-Aldrich, St. Louis, MO, USA), supplemented with fetal bovine serum (10%, Invitrogen, Carlsbad, CA, USA), penicillin (100 U/mL, Sigma-Aldrich, USA), and streptomycin (100 μg/mL, Sigma-Aldrich, USA) were applied to culture the cell lines at 37°C with 5% CO_2.

Cell transfection and treatment

Recombinant adenoviral vectors carrying HRD1 or SLC7A11 and their corresponding scrambled controls were designed and synthesized by GenePharma (Shanghai, China). When reached about 80% confluency, A2780 and SKOV3 cells were transfected with designated vectors using the Lipofectamine 2000 (Invitrogen, USA) according to the manufacturer's instructions.

Ferroptosis inhibitor, ferrostatin-1 (Fer-1) [19] and ferroptosis inducer, erastin [20] were both purchased from Selleck (Shanghai, China). After transfection with HRD1/Vector for 48 h, A2780 and SKOV3 cells were re-seeded in 24-well plates and then exposed to erastin at 20 μM or Fer-1 at 5 μM for another 24 h.

RNA extraction and quantitative real-time polymerase chain reaction (qRT-PCR)

The total RNA from OC tissues and cells was extracted using a TRIzol™ LS Reagent (Invitrogen, USA) according to the manufacturer's protocol. A total of 1 μg total RNA was reversely transcribed into complementary DNA (cDNA) with PrimeScript RT reagent Kit (Takara, Shiga, Japan) using oligo(dT) primer at 42°C for 1 h, and 2 μl the reverse transcription reaction mix was amplified by PCR with denaturation at 95°C for 2 min, followed by 50 cycles of 95°C for 30 s, 55°C for 30 s, and 72°C for 1 min. Then, qRT-PCR assay was carried out using SYBR Green PCR Kit (Takara, Japan) with the 7300 Real-Time PCR System (Applied Biosystems, Carlsbad, CA, USA). The thermocycling conditions were 94°C for 30 s, followed by 40 cycles for 94°C for 5 s, and 60°C for 30 s. Glyceraldehyde-3-phosphate dehydrogenase (GAPDH), as an internal control, was used to normalize the mRNA expressions of HRD1, glutathione peroxidase 4 (GPX4) and SLC7A11. The mRNA expression levels were quantified using $2^{-\Delta\Delta Ct}$ method. The primers for HRD1 were as follows: xF: 5′-AACCCCTGGGACAACAAGG-3′, R: 5′-GCGAGACATGATGGCATCTG-3′; the primers for GPX4 were as follows: F: 5′-TTGCCGC CTACTGAAGC-3′, R: 5′-ATGTGCCCGTCGATGT C-3′; the primers for SLC7A11 were as follows: F: 5′-GAACGAGGAGGTGGAGAAT-3′, R: 5′-ACAGG TGAAAACTCAAAGGTG-3′; the primers for GAPDH were as follows: F: 5′-AGGGCTGCTTTT AACTCTGGT-3′, R: 5′-CCCCACTTGATTTTGGA GGGA-3′.

Western blot

The cell lysates were centrifuged at 13,000 rpm for 5 min at 4°C followed by segregating by 10% sodium dodecyl sulfate polyacrylamide gel electrophoresis (SDS-PAGE). After that, the cell lysates were transferred onto polyvinylidene difluoride (PVDF) membranes purchased from Millipore (Bedford, MA, USA). A blocking buffer, bought from Sangon Biotech (Shanghai, China), was employed to block the filters for 45 min. Membranes were subsequently incubated with primary antibodies anti-HRD1 (1:1000, ab170901, Abcam, USA), anti-GPX4 (1:1000, ab125066, Abcam, USA), anti-SLC7A11 (1:1000, ab175186, Abcam, USA), anti-FTH (1:1000, ab75973, Abcam, USA), and anti-β-catenin (1:5000, ab32572, Abcam, USA) at 4°C overnight and with horseradish peroxidase-labeled secondary antibody (1:2000, ab6721, Abcam, USA) at room temperature for 2 h. Electrogenerated chemiluminescence (ECL) method was applied to visualize the protein bands.

Bromodeoxy uridine (BrdU) cell proliferation measurement

To determine the cell proliferation, the OC cell lines were seeded in a 96-well plate at a density of 5×10^3 cells per well. The proliferating cells were labeled with the supplement of a BrdU solution (10 μL/well; Sigma-Aldrich, USA) following the manufacturer's protocol. After 4 h, the cells were cultured with an anti-BrdU antibody (1:100; BioLegend, San Diego, CA, USA) at 4°C overnight.

Then, a fluorescence-conjugated secondary antibody was used to detect the cells. The stained cells were subsequently photographed with a confocal laser scanning microscope (FV1000, Olympus Corporation, Tokyo, Japan) at 200 × magnification, and the percentage of BrdU-positive cell lines was calculated. The above experiments were operated three times and analyzed from five duplicate wells.

Colony formation assay

After transfection for 48 h, cell lines were seeded in 60-mm dishes at a density of 500 cells/dish and maintained at 37°C with 5% CO_2 for 2 w. Then, paraformaldehyde (4%) was used to fix the colonies for 30 min at room temperature and crystal violet (0.1%) was subsequently used to dye them for another 30 min at room temperature. Finally, the colony cell number was counted.

Cell apoptosis assay

Annexin V Fluorescein Isothiocyanate (V-FITC) Apoptosis Detection Kit, purchased from BeiNuo Biotechnology Co., Ltd. (Shanghai, China), was employed to assess apoptotic cells. After transfection for 48 h, cell lines were harvested, washed using PBS, and resuspended in 1 × binding buffer. Next, the cell lines were stained with annexin V-FITC (5 μL) and propidium Iodide (10 μL, PI). Flow cytometry (BD FACSC Canto II, BD Biosciences, San Jose, CA, USA) was proceeded to quantify the apoptotic cells.

Malondialdehyde (MDA) assay

A Lipid Peroxidation MDA Assay Kit (Beyotime, Shanghai, China) was employed to detect the intracellular MDA content according to the manual instruction. Absorbance was determined using a microplate reader (Bio-Rad, Hercules, CA, USA) at 532 nm.

Reactive oxygen species (ROS) assay

ROS levels of OC cell lines were measured using probe 2′,7′-dichlorofluorescin diacetate (DCFH-DA, (KeyGEN, Shanghai, China). Dimethyl sulfoxide (DMSO) was used to dissolve the stock DCFH-DA (1 mM). OC cells were collected and incubated with DCFH-DA (10 μM) at 37°C for 30 min in the dark. Next, cells were washed with PBS twice and resuspended in FACS buffer. Relative DCF fluorescence intensity was determined using a flow cytometry (BD FACSC Canto II, BD Biosciences, USA).

Iron assay

An iron assay kit, bought from Abcam (ab83366), was used to detect the cellular ferrous iron content by following the manual instructions. Absorbance was determined using a microplate reader (Bio-Rad, USA) at 593 nm.

Bioinformatics analysis

UbiBrowser (http://ubibrowser.ncpsb.org/ubibrowser/home/index) [21] is an integrated bioinformatics platform that can be used to predict proteome-wide human E3-substrate networks based on naïve Bayesian networks. It currently contains 1,295 literature-reported E3–substrate interactions and 8,255 predicted E3–substrate interactions. We use it to predict the potential substrates of SLC7A11.

Co-immunoprecipitation (Co-IP)

For immunoblotting (IB) analysis, anti-FLAG antibody (GenScrip Biotech Corp, Nanjing, China), anti-HRD1 (Cell Signaling Technology, Danvers, MA, USA), anti-hemagglutinin (anti-HA, Santa Cruz Biotechnology, Dallas, TX, USA), anti-SLC7A11 (Cell Signaling Technology, USA), anti-Myc (Beijing B&M Bio Tech, Beijing, China), and anti-α-tubulin (Merck Millipore, Burlington, MA, USA) were used. For IP, TALON beads (GenScrip Biotech Corp, China) and anti-HRD1 (Abcam, USA) were used. Normal rabbit IgG (Abcam, USA) was used as the negative control. A lysis buffer, added with protease inhibitor cocktail, was contained by 150 mmol/L NaCl, 5 mmol/L Tris-base pH 8.0, 1% Nonidet-40 (NP-40), and 10% glycerin.

For co-immunoprecipitation, cells overexpressing FLAG-tagged HRD1 and HA-tagged SLC7A11 were lysed in the above lysis buffer. To remove insoluble materials, the lysate was centrifuged at 12,000 rpm for 30 min at 4°C. The TALON beads were applied to incubate the supernatants at 4°C for 3 h. Resin beads were washed five times with wash buffer which were including 25 mmol/L Tris-base (pH 8.0), 300 mmol/L NaCl, and 0.8% NP-40. Then, the TALON beads were mixed with a protein loading buffer. The mixture was subsequently boiled at 95°C for 20 min. The samples were analyzed by immunoblotting. Encoding 6 × His-tagged ubiquitin, Flag-HRD1, and HA-SLC7A1, as indicated in the figure legends, were transfected into SKOV3 cells (BeNa Culture Collection, China) using polyethylenimine (Sigma-Aldrich, USA) reagents. Cell lysates were incubated with anti-FLAG resin beads to pull down ubiquitinated proteins. After incubation for 2 h at 4°C, beads were washed 3 times with the lysis buffer, and ubiquitinated proteins were eluted with 20 µl of elution buffer (5 times SDS sample buffer, 0.05 M EDTA, and 1% SDS lysis buffer). Ubiquitination was determined by SDS-PAGE. SLC7A11 or HA antibodies were finally used to carry out western blot.

Protein half-life assay

For the SLC7A11 half-life assay, the SKOV3 cells were seeded in plates (2 cm) to approximately 60% confluence, and the cells were subsequently transfected with HRD1 or Vector plasmids. After 24 h, cells were treated with the protein synthesis inhibitor cycloheximide (CHX, 10 µg/ml; Sigma-Aldrich, USA) for the indicated duration.

In vivo tumor xenograft study

The animal study of our work was approved by the Institutional Animal Care and Use Committee of The First Affiliated Hospital of Jinzhou Medical University and carried out according to the National Institutes of Health's Guide for the Care and Use of Laboratory Animals (ethical review report number: 2022022501). Balb/c female nude mice (5–6 w, 16–20 g; 5 mice/group) were harvested from Beijing HFK Bioscience (Beijing, China) and kept under specific pathogen-free conditions (free access to sterile food and water) at 25°C for 12 h light/dark cycle. To establish OC xenograft mice models, the OC cells (SKOV3) that transfected with HRD1/Vector were collected and then suspended in sterile PBS with a density of 5×10^7 [7] cells/mL. Then, a total of 100 µL SKOV3 cell suspension liquid was subcutaneously inoculated into the ventral of the mice. The tumor length and width were examined from the first week to the fourth week post-injection using a vernier caliper. The tumor volumes were determined as follows: Tumor volume = length × width^2×0.52. At 4 w postinjection, the experimental mice were anesthetized by intraperitoneal injection with 10% chloral hydrate (60 µL) that purchased from Beyotime (Haimen, China) and subsequently sacrificed by cervical dislocation. No multiple tumors were present. The heartbeat of all the mice had stopped. After confirming that, the tumors were collected, weighed, and photographed.

Statistical analysis

SPSS 19.0 (IBM, USA) was performed to carry out statistical analysis. The data were expressed as the mean ± standard deviation (SD). For comparison between two groups, unpaired Student's t-test was used for the data of normal distribution, while Mann–Whitney test was used for data of non-Gaussian distribution. One-way analysis of variance (ANOVA) with Tukey's post hoc test was used to compare the differences between more than two groups. P-values <0.05 were considered statistically significant.

Results

HRD1 was downregulated in OC tissues

First, the expression levels of HRD1 in 15 cases of OC tumor tissue samples and 15 cases of nonmalignant ovarian tissue samples were measured using qRT-PCR. As shown in Figure 1a, the

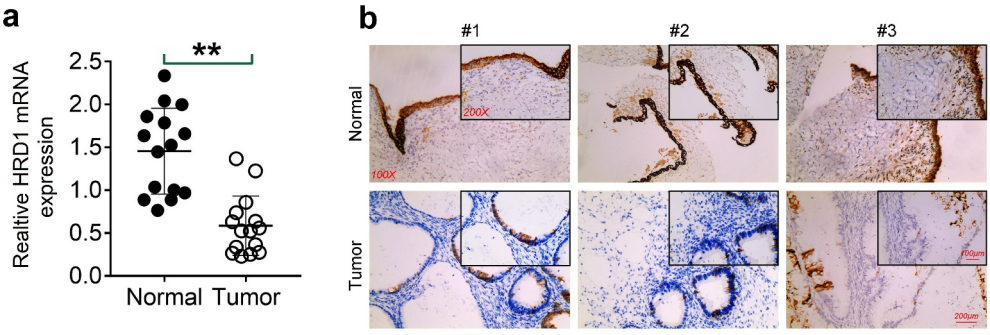

Figure 1. HRD1 was downexpressed in OC tumor tissues. (a) The expression of HRD1 in 15 cases of OC tumor tissue samples and 15 cases of nonmalignant ovarian tissue samples were detected using qRT-PCR. (b) Representative images of immunohistochemical staining of tissues with HRD1 antibody (×200). Data were shown as mean ± SD. $^{**}P<0.01$ vs Normal group.

expression level of HRD1 in OC tumor tissue samples was significantly lower than that in nonmalignant ovarian tissue samples ($P<0.01$). Images from IHC also confirmed that HRD1 was downregulated in OC tumor samples when compared to that in nonmalignant ovarian tissue samples (Figure 1b). As shown in Table 1, HRD1 level was correlated with tumor staging and lymphatic metastasis. These results indicated that HRD1 might be a novel biomarker for predicting the malignant progression of OC.

The overexpression of HRD1 inhibited OC cell proliferation in vitro *and tumor growth* in vivo

To explore the effect of HRD1 on OC cell proliferation, the HRD1 overexpression plasmids were constructed and transfected into human OC cell lines A2780 and SKOV3. Western blot confirmed the transfection efficiency of HRD1 overexpression in both A2780 and SKOV3 cell lines ($P<0.01$, Figure 2a). Then, the cell proliferation of A2780 and SKOV3 cells was detected using BrdU assay. As shown in Figure 2b, in A2780 and SKOV3 cell lines, the BrdU-positive cell numbers in vector groups were both remarkably higher than that in HRD1 groups ($P<0.01$). Besides, cell colony formation assay was carried out to observe the cell colony formation. Obviously, the colony cell numbers of vector groups were both higher than that of HRD1 groups ($P<0.01$, Figure 2c). Next, OC nude mice models were established to explore the effect of HRD1 on OC tumor growth *in vivo*. Results from animal experiments displayed that the overexpression of HRD1 markedly inhibited OC tumor size, weight, and volume *in vivo* ($P<0.01$, Figure 2d). These data proved that the upregulation of HRD1-suppressed OC cell proliferation and colony formation *in vitro* and repressed OC tumor growth *in vivo*.

The overexpression of HRD1 promoted ferroptosis in OC cell lines

Flow cytometry was performed to assess cell apoptosis. As shown in Figure 3a, HRD1 transfection significantly increased cell apoptosis in both A2780 and SKOV3 ($P<0.01$). To further explore the effect of HRD1 overexpression on ferroptosis in OC cells, the contents of ferroptosis-related indicators (ROS and MDA) in experimental OC cells were detected using the corresponding commercial kits, and the relative DCF fluorescent intensity was considered to express the content of ROS. Obviously, the contents of ROS and MDA in HRD1 groups were both higher than that in Vector groups ($P<0.01$, Figure 3b). Then, the transfected cell lines were co-treated with Erastin or Fer-1 to promote or inhibit ferroptosis. Data from flow cytometry also showed that the apoptosis caused by HRD1 overexpression and/or Erastin treatment was completely offset by FER-1 treament ($P<0.01$, Figure 3c). Besides, the contents of ferroptosis-related indicators (ROS, MDA, and Fe^{2+}) were measured using the corresponding commercial kits. The increases of the ROS, MDA, and Fe^{2+} contents that caused by HRD1 overexpression and/or Erastin treatment were also completely recovered by FER-1 treament ($P<0.01$, Figure 3d). These above data illustrated that the

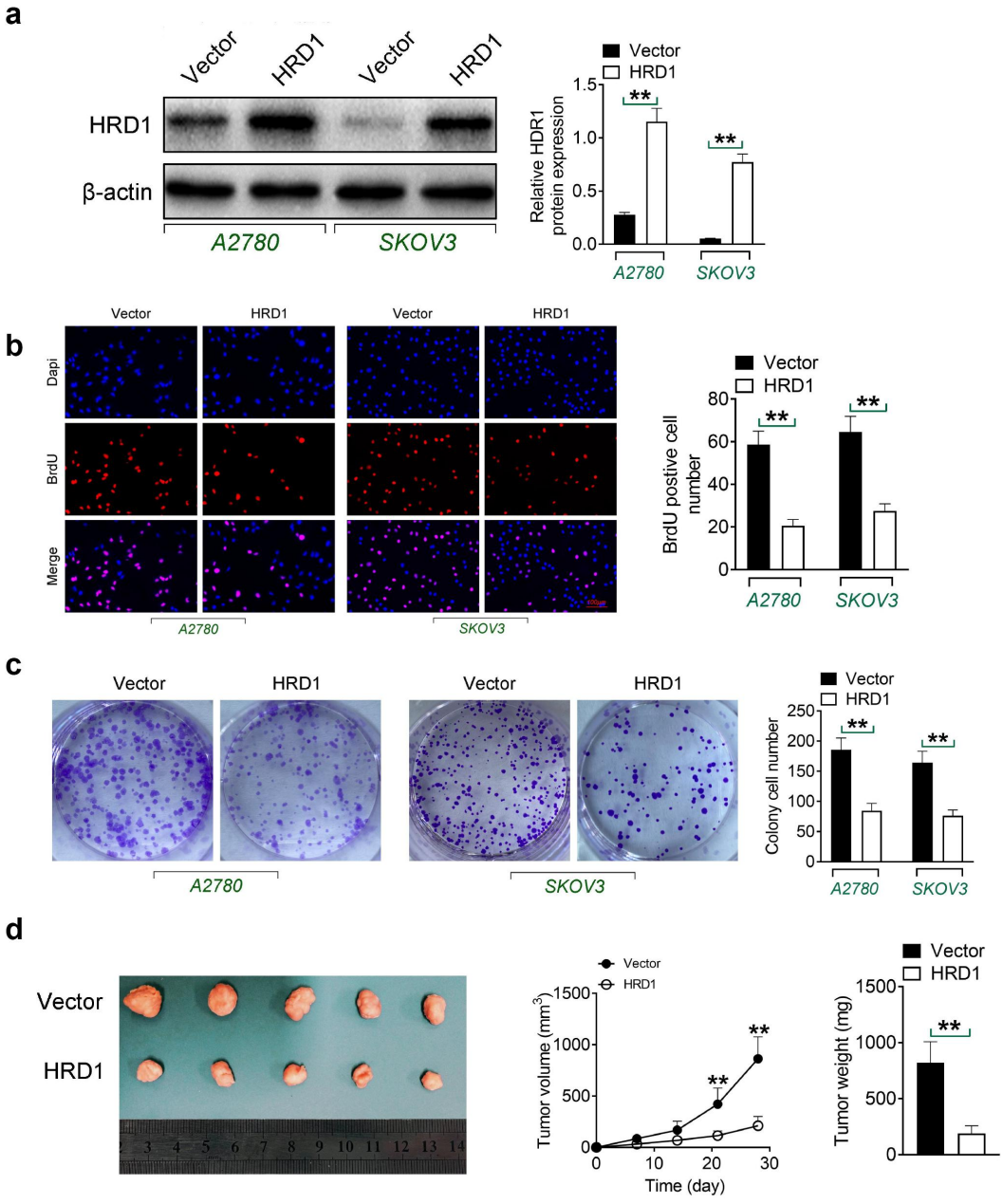

Figure 2. The overexpression of HRD1 inhibited OC cell proliferation and tumor formation. (a) the efficiency of transfection was examined using western blot. (b) The cell proliferation was detected using BrdU assay. (c) The cell colony formation was assessed using cell colony formation assay. (d) The tumor size, weights, and volumes of OC mice models were measured and recorded. Data were shown as mean ± SD. $^{**}P<0.01$ vs Vector groups.

overexpression of HRD1 enhanced ferroptosis in OC cell lines.

HRD1 regulated the stability of SLC7A11 in OC cell lines

To further define the correlation between HRD1 and ferroptosis in OC cell lines, the mRNA and protein expressions of ferroptosis-related factors (GPX4, SLC7A11, and FTH) were, respectively, measured using qRT-PCR and western blot. Data from qRT-PCR exhibited that there was no significant difference in the mRNA expression of GPX4, SLC7A11, and FTH between the Vector groups and HRD1 groups in A2780 or SKOV3 cell lines (Figure 4a). However, data from western blot showed that the protein

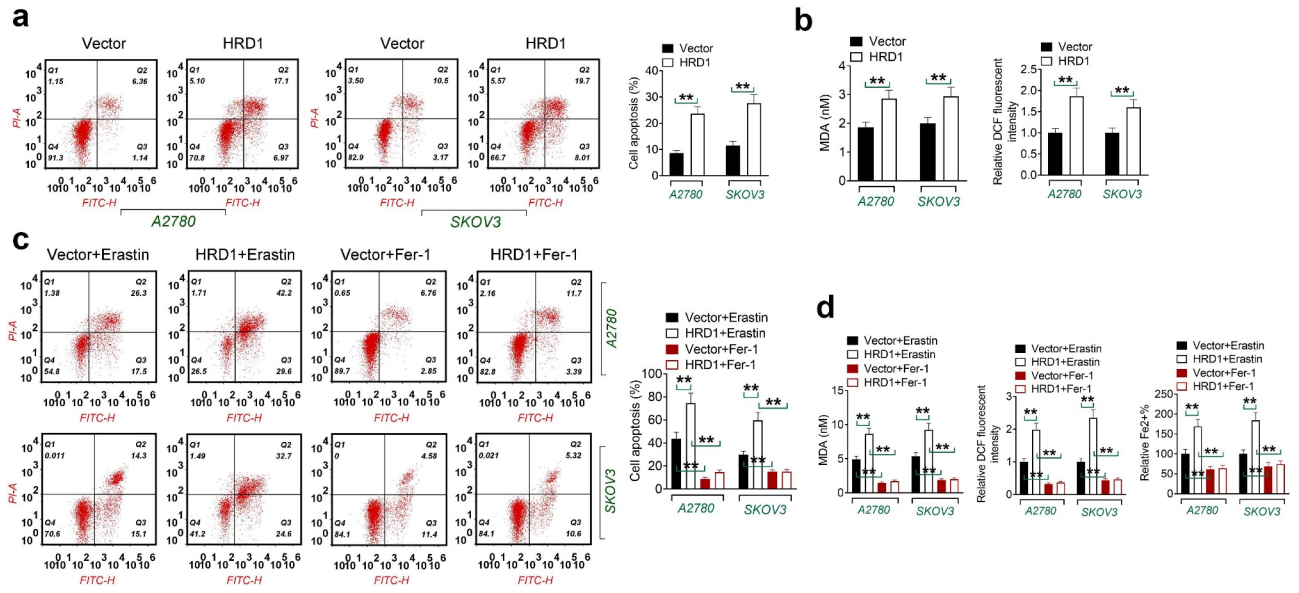

Figure 3. The overexpression of HRD1 promoted ferroptosis in OC cells. (a) The cell apoptosis was detected using flow cytometry. (b) The contents of MDA and ROS were assessed using corresponding commercial kits. (c) The cell apoptosis was detected using flow cytometry. (d) The contents of MDA, ROS, and Fe^{2+} were assessed using corresponding commercial kits. Data were shown as mean ± SD. ***P*<0.01 vs Vector groups, Vector+Erastin or Vector+Fer-1 groups.

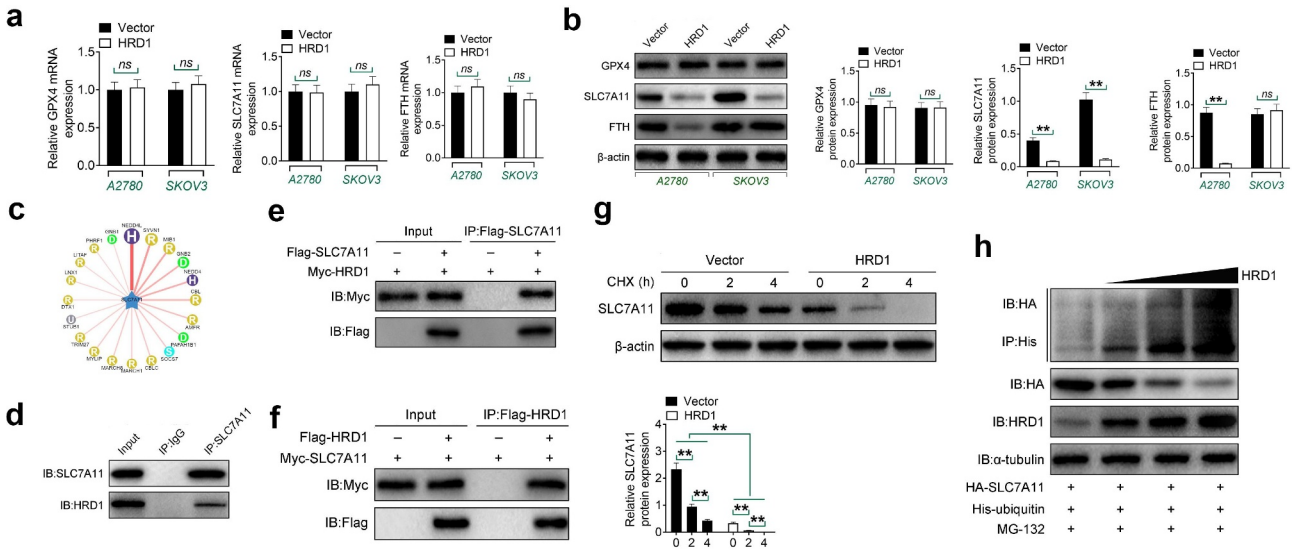

Figure 4. HRD1 regulated the stability of SLC7A11. (a) The mRNA expressions of GPX4, SLC7A11 and FTH were detected using qRT-PCR. (b) The protein expressions of GPX4, SLC7A11 and FTH were detected using western blot. The combination between HRD1 and SLC7A11 was predicted and verified using UbiBrowser (c) and Co-IP assay (d, e and f), respectively. (g) The stability of SLC7A11 was analyzed using protein half-life assay. (h) The ubiquitination of SLC7A11 was measured using Co-IP assay. Data were shown as mean ± SD. ***P*<0.01 vs Vector groups.

expressions of SLC7A11 expression of Vector groups were significantly higher than that of HRD1 groups in both A2780 and SKOV3 cell lines (*P*<0.01), and the FTH expression of Vector group was remarkably higher than that of HRD1 group in A2780 cell lines (*P*<0.01), while it had no significant difference between Vector group and HRD1 group in SKOV3 cell lines (Figure 4b). The combination of HRD1 and SLC7A11 was predicted and verified via online bioinformatics tool UbiBrowser (http://ubibrowser.ncpsb.org/ubibrowser/home/index) (Figure 4d) and Co-IP assay, respectively (Figure 4d–f). The endogenous

SLC7A11 protein was co-precipitated by an HRD1-specific antibody, while endogenous HRD1 was co-precipitated by an SLC7A11-specific antibody (Figure 4d–f). Half-time assay was subsequently carried out to test the stability of SLC7A11 in OC cell lines. The half-life of SLC7A11 was examined in the presence or absence of HRD1. We treated SKOV3 cells with or without HRD1 overexpression with CHX and examined SLC7A11 expression levels at 0 h, 2 h, and 4 h. The half-life of endogenous SLC7A11 was markedly shortened in the SKOV3 cell lines with HRD1 overexpression ($P < 0.01$, Figure 4g). To explain the mechanism by which HRD1 stabilized SLC7A11, we defined whether HRD1 directly modulated the levels of SLC7A11 ubiquitination. As shown in Figure 4h, we co-expressed the increasing amounts of Flag-tagged HRD1 with His-tagged ubiquitin and HA-SLC7A11. TALON beads were employed to pull down ubiquitinated proteins, followed by the measurement of SLC7A11 via the HA antibody, and Figure 4h shows that the ubiquitination of SLC7A11 was dose-dependently induced by HRD1. These results suggested that HRD1 interacted with SLC7A11, reduced its stability, and stimulated its ubiquitination.

SLC7A11 overexpression eliminated the effect of HRD1 overexpression on OC cell lines

To further verify the interaction between HRD1 and SLC7A11 in OC cell lines, SKOV3 cell lines were divided into four groups (Vector, HRD1, HRD1 + NC, and HRD1 + SLC7A11) according to different treatments. Images from BrdU assay and cell colony formation assay, respectively, showed that the inhibition of cell proliferation and colony formation caused by HRD1 overexpression was significantly abrogated via the overexpression of SLC7A11 ($P<0.01$, Figure 5a,b). Data from flow cytometry showed that the increase of cell apoptosis which was resulted from HRD1 overexpression was obviously reduced by SLC7A11 overexpression ($P<0.01$, Figure 5c). In addition, as shown as Figure 5d, the enhancement of ferroptosis (ROS, MDA, and Fe^{2+}) induced by HRD1 overexpression was also repressed with SLC7A11 upregulation ($P<0.01$). These data showed that SLC7A11 overexpression recovered the effect of HRD1 overexpression on OC cell lines.

Discussion

Growing evidence indicates that ferroptosis participates in regulating cancer progression [22,23]. Here, we identified that elevated expression of HRD1 serves as a ferroptosis promoter and inhibited OC growth and metastasis. Furthermore, HRD1 downregulated SLC7A11 by promoting SLC7A11 degradation in OC cells, thereby inducing ferroptosis and inhibiting OC progression.

Since the pathogenesis of OC is very complex, the understanding of the progression of OC is still limited. In recent years, extensive studies have revealed multifarious regulators in OC

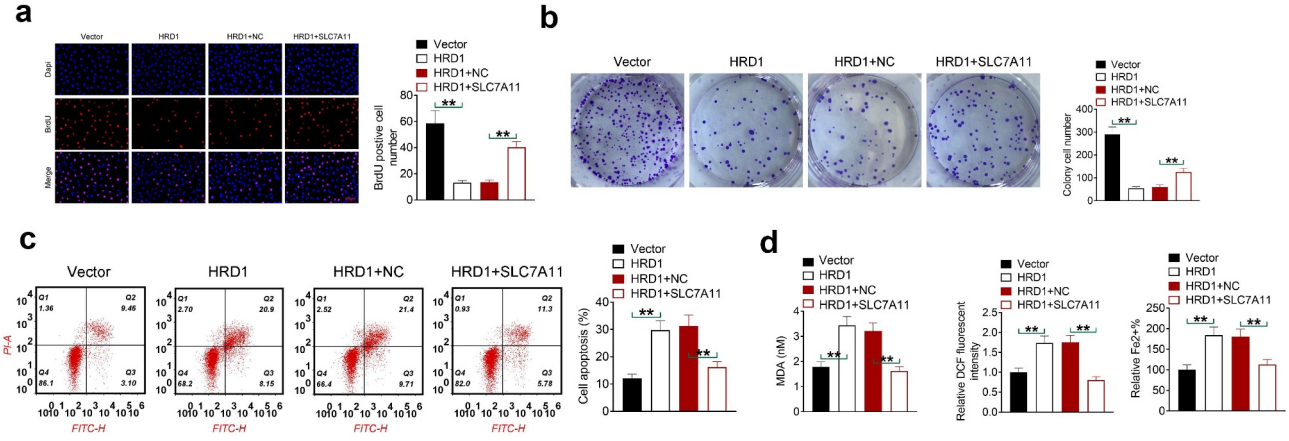

Figure 5. The overexpression of SLC7A11 eliminated the effect of HRD1 overexpression on OC cells. (a) The cell proliferation was detected using BrdU assay. (b)The cell colony formation was assessed using colony formation assay.(c) The cell apoptosis was detected using flow cytometry. (d) The contents of MDA and ROS were assessed using corresponding commercial kits.Data were shown as mean ± SD. **$P<0.01$ vs Vector groups or HRD1+NC groups.

progression, which might be used as prognostic indicators for the treatment target of OC. For instance, the downregulation of ribosomal protein S6 (RPS6) inhibited cell activities in epithelial OC cell lines through blocking cells in G0/G1 phase [24]. Yang *et al.* found that transcriptional coactivator with PDZ-binding motif (TAZ) mediated a cell density-regulated ferroptosis in OC by modulating angiopoietin-like 4 (ANGPTL4)-NADPH oxidase 2 (NOX2) axis [25]. HRD1, as an E3 ubiquitin ligase, plays an essential role in the ubiquitination and dislocation of misfolded protein in ERAD [11,12]. In various types of cancer, the expression of HRD1 is dysregulated, and it targets different molecules to develop cancer hallmarks or suppress the cancer progression [26]. However, its role in OC proliferation and ferroptosis is unclear. In this study, we show that HRD1 was downregulated in OC tissues based on qRT-PCR and IHC analysis. We also showed that HRD1 expression was inversely correlated with tumor stage and metastasis of OC patients. These results indicate that HRD1 is a potential biomarker for OC. Furthermore, we demonstrated that HRD1 ectopic expression inhibited the proliferation and colony formation of OC cells while inducing apoptosis. *In vivo*, overexpression of HRD1 inhibited tumor growth. These findings suggest that HRD1 may act as a tumor suppressor in OC.

Ferroptosis is a non-apoptotic form of cell death caused by the accumulation of toxic lipid peroxidation, and the accumulation of intracellular ROS is one of the direct causes of ferroptosis [27,28]. As a key regulator of ferroptosis, SLC7A11 can be regulated by a variety of upstream factors, and is involved in the progression of OC. For example, Hong et al. showed that PARP inhibition promotes the ferroptosis in BRCA-mutant OC via downregulating SLC7A11 [29]. Cai et al. reported that long noncoding RNA ADAMTS9-AS1 attenuates ferroptosis by targeting miR-587/SLC7A11 axis in OC [9]. Jin et al. demonstrated that SNAI2 directly binds to SLC7A11 promoter and regulate SLC7A11 expression, thereby promoting the development of OC by inducing ferroptosis [10]. The existing data in this study illustrated the promotive effect of HRD1 overexpression on ferroptosis in OC cells. In our work, the potential-binding relationship between HRD1 and SLC7A11 promoter was disclosed by a bioinformatics analysis from UbiBrowser (http://ubibrowser.ncpsb.org/ubibrowser/home/index), which was further verified by the Co-IP assay. In addition, HRD1 upregulation remarkably repressed the protein expression of SLC7A11. Mechanistically, HRD1 catalyzed SLC7A11 ubiquitination and promoted SLC7A11 degradation. Furthermore, the antitumor and pro-ferroptosis effects of HRD1 overexpression on OC cells *in vitro* were partially weakened by SLC7A11 overexpression, further verifying the critical role of HRD1-mediated ferroptosis in OC progression. Anyway, we acknowledged some limitations in this study. Further studies are warranted to further validate these findings in a larger cohort of OC patients. Furthermore, it is still unclear whether the regulatory effect of HRD1 on SLC7A11 expression is directly determined by their direct-binding relationship or through indirect inhibition of SLC7A11 expression. Further studies will also examine the effect of HRD1 on other key regulators in OC progression.

In conclusion, our paper demonstrated that HRD1 suppressed tumorigenesis and development of OC by promoting ferroptosis. Moreover, HRD1 could directly bind to SLC7A11 promoter and regulate SLC7A11 expression, which might be the potential mechanism underlying HRD1-regulated ferroptosis in OC. Our findings elucidated the molecular mechanism of ferroptosis-mediated OC and provided targets for OC treatments.

Disclosure statement

No potential conflict of interest was reported by the authors.

Funding

This study was supported by the Natural Science Foundation Project of Liaoning Province (20180551264), the Youth Project of Education Department of Liaoning Province (JYTQN2020034), and Transverse research projects of Jinzhou Medical University (Grant No. H2022036)

Availability of data and materials

The data sets used and/or analyzed during the current study are available from the corresponding author on reasonable request.

References

[1] Stewart C, Ralyea C, Lockwood S. Ovarian Cancer: an integrated review. Semin Oncol Nurs. 2019;35(2):151–156.

[2] Matulonis UA, Sood AK, Fallowfield L, et al. Ovarian cancer. Nat Rev Dis Primers. 2016;2(1):16061.

[3] Sung H, Ferlay J, Siegel RL, et al. Global cancer statistics 2020: gLOBOCAN estimates of incidence and mortality worldwide for 36 cancers in 185 Countries. CA Cancer J Clin. 2021;71(3):209–249.

[4] Cortez AJ, Tudrej P, Kujawa KA, et al. Advances in ovarian cancer therapy. Cancer Chemother Pharmacol. 2018;81(1):17–38.

[5] Li J, Cao F, Yin HL, et al. Ferroptosis: past, present and future. Cell Death Amp Dis. 2020;11(2):88.

[6] Li L, Qiu C, Hou M, et al. Ferroptosis in ovarian cancer: a novel therapeutic strategy. Front Oncol. 2021;11:665945.

[7] Koppula P, Zhuang L, Gan B. Cystine transporter SLC7A11/xCT in cancer: ferroptosis, nutrient dependency, and cancer therapy. Protein Cell. 2021;12(8):599–620.

[8] Ke Y, Chen X, Su Y, et al. Low expression of SLC7A11 confers drug resistance and worse survival in ovarian cancer via inhibition of cell autophagy as a competing endogenous RNA. Front Oncol. 2021;11:744940.

[9] Cai L, Hu X, Ye L, et al. Long non-coding RNA ADAMTS9-AS1 attenuates ferroptosis by Targeting microRNA-587/solute carrier family 7 member 11 axis in epithelial ovarian cancer. Bioengineered. 2022;13(4):8226–8239.

[10] Jin Y, Chen L, Li L, et al. SNAI2 promotes the development of ovarian cancer through regulating ferroptosis. Bioengineered. 2022;13(3):6451–6463.

[11] Schulz J, Avci D, Queisser MA, et al. Conserved cytoplasmic domains promote Hrd1 ubiquitin ligase complex formation for ER-associated degradation (ERAD). J Cell Sci. 2017;130:3322–3335.

[12] Kawaguchi K, Yamamoto-Hino M, Murakami Y, et al. Hrd1-dependent degradation of the unassembled PIGK subunit of the GPI transamidase complex. Cell Struct Funct. 2021;46(2):65–71.

[13] Fan Y, Wang J, Jin W, et al. CircNR3C2 promotes HRD1-mediated tumor-suppressive effect via sponging miR-513a-3p in triple-negative breast cancer. Mol Cancer. 2021;20(1):25.

[14] Fan Y, Wang J, Xu Y, et al. Anti-Warburg effect by targeting HRD1-PFKP pathway may inhibit breast cancer progression. Cell Commun Signal. 2021;19(1):18.

[15] Guo X, Wang A, Wang W, et al. HRD1 inhibits fatty acid oxidation and tumorigenesis by ubiquitinating CPT2 in triple-negative breast cancer. Mol Oncol. 2021;15(2):642–656.

[16] Tan X, He X, Fan Z. Upregulation of HRD1 promotes cell migration and invasion in colon cancer. Mol Cell Biochem. 2019;454(1–2):1–9.

[17] Liu L, Yu L, Zeng C, et al. E3 ubiquitin ligase HRD1 promotes lung tumorigenesis by promoting sirtuin 2 ubiquitination and degradation. Mol Cell Biol. 2020;40(7):40.

[18] Li AM, Lin XW, Shen JT, et al. HRD1 attenuates the high uptake of [(18)F]FDG in hepatocellular carcinoma PET imaging. Nucl Med Biol. 2021;96-97:27–34.

[19] Ito K, Eguchi Y, Imagawa Y, et al. MPP+ induces necrostatin-1- and ferrostatin-1-sensitive necrotic death of neuronal SH-SY5Y cells. Cell Death Discov. 2017;3(1):17013.

[20] Zhang Y, Tan H, Daniels JD, et al. Imidazole ketone erastin induces ferroptosis and slows tumor growth in a mouse lymphoma model. Cell Chem Biol. 2019;26(5):623–33 e9.

[21] Wang X, Li Y, He M, et al. UbiBrowser 2.0: a comprehensive resource for proteome-wide known and predicted ubiquitin ligase/deubiquitinase-substrate interactions in eukaryotic species. Nucleic Acids Res. 2022;50:D719–28.

[22] Zhang C, Liu N. Ferroptosis, necroptosis, and pyroptosis in the occurrence and development of ovarian cancer. Front Immunol. 2022;13:920059.

[23] Lei G, Zhuang L, Gan B. Targeting ferroptosis as a vulnerability in cancer. Nat Rev Cancer. 2022;22(7):381–396.

[24] Yang X, Xu L, Yang YE, et al. Knockdown of ribosomal protein S6 suppresses proliferation, migration, and invasion in epithelial ovarian cancer. J Ovarian Res. 2020;13(1):100.

[25] Yang WH, Huang Z, Wu J, et al. A TAZ–ANGPTL4–NOX2 axis regulates ferroptotic cell death and chemoresistance in epithelial ovarian cancer. Mol Cancer Res. 2020;18(1):79–90.

[26] Karamali N, Ebrahimnezhad S, Khaleghi Moghadam R, et al. HRD1 in human malignant neoplasms: molecular mechanisms and novel therapeutic strategy for cancer. Life Sci. 2022;301:120620.

[27] Ma TL, Chen JX, Zhu P, et al. Focus on ferroptosis regulation: exploring novel mechanisms and applications of ferroptosis regulator. Life Sci. 2022;307:120868.

[28] Yan HF, Zou T, Tuo QZ, et al. Ferroptosis: mechanisms and links with diseases. Signal Transduct Target Ther. 2021;6(1):49.

[29] Hong T, Lei G, Chen X, et al. PARP inhibition promotes ferroptosis via repressing SLC7A11 and synergizes with ferroptosis inducers in BRCA-proficient ovarian cancer. Redox Biol. 2021;42:101928.